Supporting Information

Chan et al. 10.1073/pnas.0914585107

SI Materials and Methods

Materials. Human collagen IV, human collagen I, and Matrigel growth factor reduced LDEV free were purchased from BD Biosciences. Soybean lecithin was purchased from Alfa Aeser. 1,2-Distearoyl-sn-Glycero-3-Phosphoethanolamine-*N*-[Maleimide (PolyethyleneGlycol) 2000] (ammonium salt) (DSPE-PEG-maleimide) and 1,2-Distearoyl-sn-Glycero-3-Phosphoethanolamine-N-[Methoxy (PolyethyleneGlycol) 2000] (ammonium salt) (DSPE-PEG) were purchased from Avanti Polar Lipids. Poly ($_{D,L}$-lactic-*co*glycolic acid) (PLGA) polymers (inherent viscosity: 0.19 dL/g) were purchased from Durect Corporation. All peptides were custom synthesized by GenScript with C-terminal amidation and purified by RP-HPLC to >95% purity by mass spectral analysis. Peptides were synthesized with a linker sequence (GGGC) at the C terminus for maleimide-thiol coupling. Alexa Fluor 647 hydrazide Tris(triethylammonium) salt was purchased from Invitrogen.

Matrigel Binding Studies. Ninety-six-well plates were coated with 100 μL 1/50 dilutions of Matrigel in TBS overnight at 4 °C or TBS buffer only. Plates were blocked with 3% BSA/TBS for 2 h at RT and washed three times; 10^{10} pfu of each phage clone was added in 0.5% TBST in triplicate to either Matrigel or BSA-coated wells. Bound phage particles were detected with peroxidase-conjugated mouse anti-M13 monoclonal antibodies (mAb) at 1/5,000 dilution (Amersham). After a 1 h incubation, the reaction was developed with 2,2′-azino-bis(3-ethylbenzthiazoline-6-sulphonic acid) (ABTS) (Amersham) and the absorbance was read at 405 nm against a reference wavelength of 490 nm with a SpectraMax Plus 384 microplate reader (Molecular Devices).

IC_{50} Value Determination of Phage Clones. Matrigel-coated and blocked 96-well plates were incubated in triplicate with 10^{-5}–10^{-10} M peptide concentrations and 10^9 pfu of phage in 100 μL 0.5% TBST. After 1 h at RT, bound phages were labeled with anti-M13 mAbs and color was developed and detected by ABTS absorbance (405–490 nm). Peptide inhibition curves were normalized on a percentage scale. IC_{50} values were calculated using a dose–response curve fit by the formula: Y = Bottom + (Top − Bottom)/(1 + 10^[(LogIC_{50} − X)*HillSlope)] (Origin 8 data analysis software).

Release Kinetics Studies. To assess the Ptxl–PLA bond, Ptxl and Ptxl–PLA conjugates were subject to RP-HPLC using an Agilent 1100 HPLC equipped with a pentafluorophenyl column (Curosil-PFP, 250 × 4.6 mm, 5 μm; Phenomenex). Ptxl and Ptxl–PLA absorbance was measured with an UV–Vis detector at 227 nm in a 1/1 acetonitrile/1% trifluoroacetic acid 1 mL/min nongradient mobile phase. To quantify the Ptxl–PLA drug release profile, a 2-mg nanoburr sample was divided equally into Slide-A-Lyzer MINI dialysis microtubes with a molecular weight cutoff of 20,000 Da (Pierce). The remaining Ptxl–PLA was quantified at various time points by RP-HPLC. Experiments were carried out in triplicate in PBS at 37 °C.

Optical Imaging and Fluorescence Microscopy Studies. Tissues were fixed in 4% paraformaldehyde/4% sucrose/saline overnight at 4 °C. Whole tissue sections were imaged simultaneously using the IVIS Imaging System 200 Series at 640/700 (ex/em) wavelength, exposure time = 1 s, binning = medium, F/Stop = 2. Tissue sections were overlayed onto photographs taken at binning = medium, F/Stop = 8. After IVIS imaging, the same tissues were OCT-frozen and cut to give approximately 10-μM sections for fluorescent microscopy. Representative H&E stained slides were made from paraffin-fixed sections. All histology sections were done by Massachusetts Institute of Technology Koch Institute Histology Facility and imaged using a DeltaVision RT deconvolution microscope using the 10× or 20× objective (Applied Precision Inc.).

Statistical Analysis. Student's *t* test or one-way ANOVA with post hoc Tukey tests were used to determine significance. All error bars represent the SD of the mean.

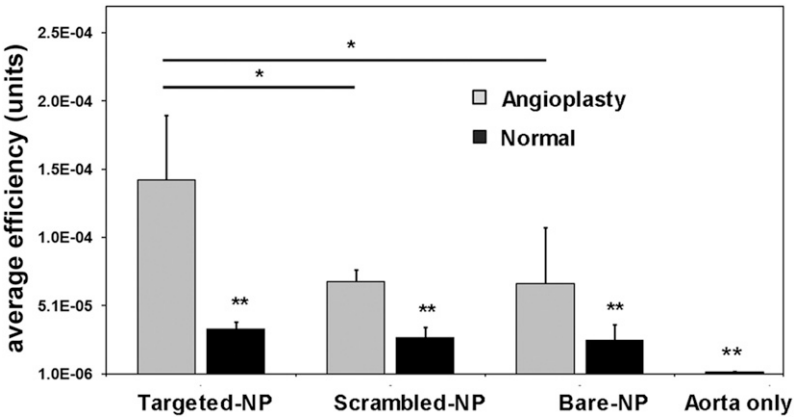

Fig. S1. Quantification of nanoburr binding ex vivo to angioplastied aortas. Aorta sections ($n = 3$) were analyzed using the region-of-interest (ROI) function of the IVIS Living Image Software. Values are shown here as average fluorescence efficiency (rfu) (mean ± SD). Aorta-only sections did not have nanoparticles delivered into them. *, $P < 0.05$, **, $P < 0.01$ by one-way analysis of variance with Tukey post hoc test.

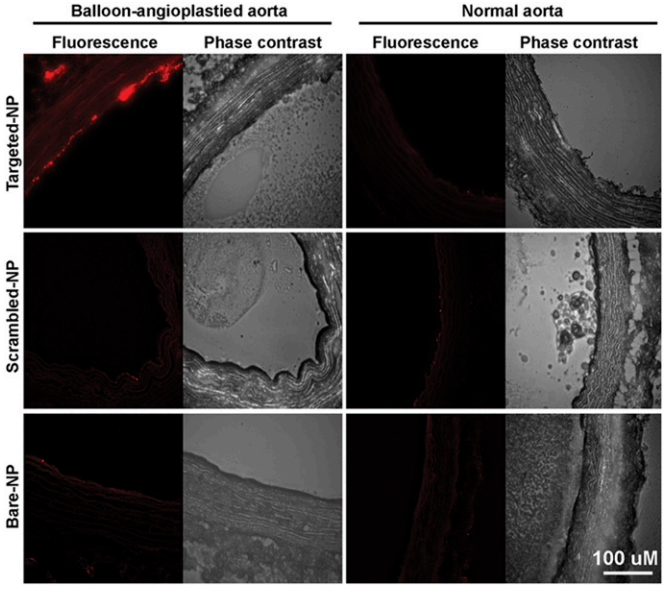

Fig. S2. Representative images of nanoburr binding to angioplastied and normal aortas ex vivo. (*Top*) Fluorescence and phase contrast images of aortas incubated with nanoburrs. (*Middle*) Aortas incubated with scrambled-peptide NPs. (*Bottom*) Aortas incubated with nontargeted NPs. (Scale bar, 100 μm.) Images were obtained with a DeltaVision deconvolution microscope using the 20× objective.

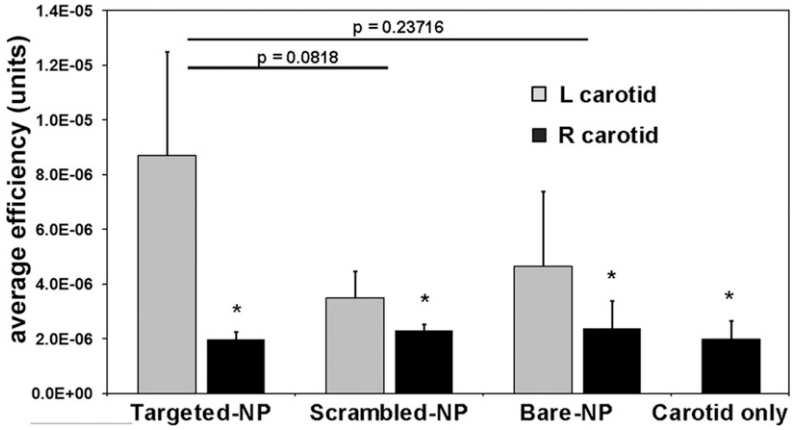

Fig. S3. Quantification of nanoburr binding in vivo to angioplastied left common carotids by IA delivery. Both the left and right common carotid arteries ($n = 3$) were analyzed using the ROI function of the IVIS Living Image Software. Values are shown here as average fluorescence efficiency (rfu) (mean ± SD). Carotid-only sections did not have nanoparticles delivered into them. *, $P < 0.05$ by one-way analysis of variance with Tukey post hoc test.

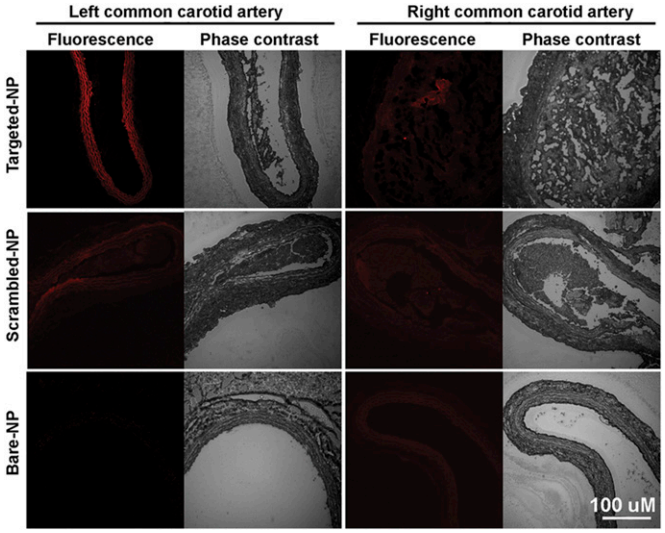

Fig. S4. Representative images of nanoburr binding in vivo by IA delivery to angioplastied left common carotids. (*Top*) Fluorescence and phase contrast images of carotid arteries incubated with nanoburrs. (*Middle*) Carotid arteries incubated with scrambled-peptide NPs. (*Bottom*) Carotid arteries incubated with nontargeted NPs. (Scale bar, 100 μm.) Images were obtained with a DeltaVision deconvolution microscope using the 20× objective.

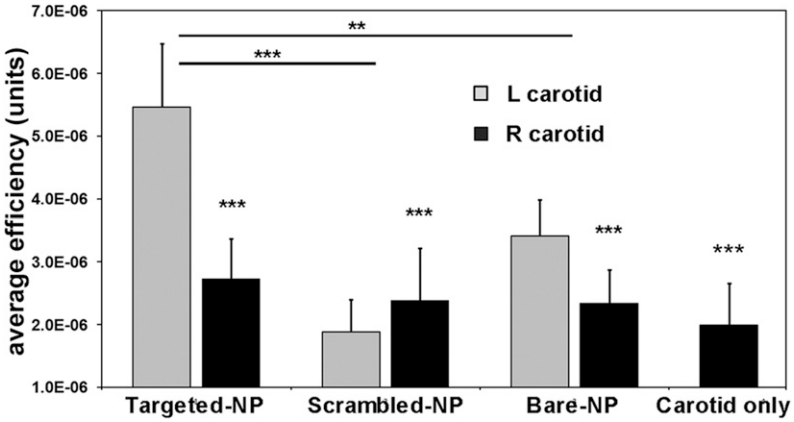

Fig. S5. Quantification of nanoburr binding in vivo to angioplastied left common carotids by i.v. delivery. Both the left and right common carotid arteries ($n = 5$) were analyzed using the ROI function of the IVIS Living Image Software. Values are shown here as average fluorescence efficiency (rfu) (mean ± SD). Carotid-only sections did not have nanoparticles delivered into them. **, $P < 0.01$; ***, $P < 0.001$ by one-way analysis of variance with Tukey post hoc test.

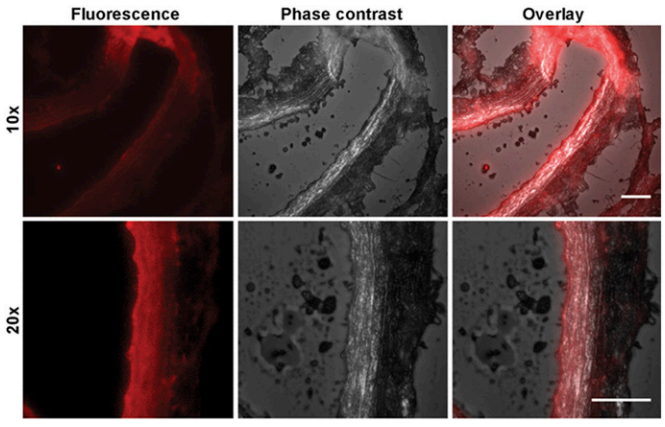

Fig S6. Representative images of nanoburr binding in vivo by i.v. delivery to angioplastied left common carotids. (*Left* to *Right*) fluorescence, phase contrast and overlay images of angioplastied left common carotid arteries incubated with nanoburrs at 10× and 20× magnification. (Scale bar, 100 μm.) Images were obtained with a DeltaVision deconvolution microscope using the 10× and 20× objective.